Impact of IBR Control on the Performance of Under-Frequency Load Shedding Scheme

Xinquan Chen[1], Aboutaleb Haddadi[3], Evangelos Farantatos[3], Ilhan Kocar[2]

1. Department of Electrical and Electronic Engineering, The Hong Kong Polytechnic University, Hong Kong SAR, China.

2. Polytechnique Montreal, Montreal, QC H3T 1J4, Canada.

3. Electric Power Research Institute (EPRI), Palo Alto, CA 94301 USA.

e-mail: ilhan.kocar@polymtl.ca

***Abstract*− Under-frequency load shedding (UFLS) operation depends on system inertia among other factors. The increasing adoption of inverter-based resources (IBRs) coupled with declining synchronous generator (SG) deployment reduces system inertia. This reduction can impact system response during under-frequency events, potentially impacting the performance of the UFLS scheme. This phenomenon has been investigated in existing studies for low-bandwidth IBR control. Using EMT simulations of a modified North American transmission system, we demonstrate that high-bandwidth IBR control can support the proper operation of UFLS in contrast to conventional low-bandwidth IBR control. This improvement stems from the fast injection of active power by high-bandwidth IBR control in response to frequency decline, provided there is sufficient energy capacity to compensate for generator loss. Our analysis reveals that IBR control parameters influence UFLS scheme effectiveness, informing future coordination between IBR control and UFLS schemes.**

***Keywords*: Inverter-based resource, EMT, protection, under-frequency load shedding.**

I. Introduction

Under-frequency load shedding (UFLS) is a protection scheme that reduces generation-load imbalance following generation losses [1]. By monitoring system frequency and disconnecting predetermined loads when frequency falls below specified thresholds [2], UFLS helps prevent system-wide blackouts and protects generators from sustained low-frequency operation.

The effectiveness of UFLS schemes depends on system inertia, among other factors [4], [5]. As power systems transition from synchronous generators (SGs) to inverter-based resources (IBRs) with no inherent rotational inertia, system inertia decreases because IBRs lack the rotating components that enable SGs to supply kinetic energy through their spinning rotors [6], [7]. Conventional low-bandwidth IBR control, hereinafter referred to as grid-following, exhibits frequency responses distinct from SGs, potentially resulting in higher rate-of-change-of-frequency (RoCoF) [8]. These higher RoCoF values lead to deeper frequency excursions, potentially triggering excessive load shedding by UFLS schemes [9]. Such excessive load shedding can cause over-frequency conditions and subsequent generation tripping [10]; potentially cascading into area-wide blackouts.

High-bandwidth IBR control, hereinafter referred to as grid-forming, can provide grid services which may address those challenges. The literature has presented a number of generic high-bandwidth primary control strategies, including virtual synchronous machine (VSM) control, droop control, and dispatchable virtual oscillator control (dVOC) [11], [12]. These high-bandwidth IBRs can provide fast frequency support through power-synchronization loops (PSLs), demonstrating a wider range of frequency regulation services compared to low-bandwidth IBRs [13]. However, high-bandwidth IBR performance depends on control strategies and parameter tuning, as these factors determine frequency response and output impedance [14]. Improper control settings can degrade system dynamic performance as high-bandwidth IBR penetration increases, compromising frequency resilience.

It is important to note that both low-bandwidth and high-bandwidth IBRs can provide frequency support services. However, high-bandwidth control is generally more favorable for supporting UFLS operation due to its higher control bandwidth compared to low-bandwidth control [3]. The reason is that in a low-bandwidth IBR, frequency support controls are typically implemented at plant level, which results in a slower response time compared to unit-level control. This delay may limit the effectiveness of a low-bandwidth IBR in supporting UFLS operation, where rapid response is needed. By contrast, a high-bandwidth IBR usually implements frequency support controls at inverter unit level, enabling a faster response time that aligns with the operational time frame of a UFLS scheme. Reference [3] has shown that plant-level primary frequency regulation (PFR) by a low-bandwidth IBR may not support UFLS, whereas unit-level PFR by a high-bandwidth IBR can support UFLS.

Recent research has explored several aspects of UFLS in modern power systems, including novel UFLS methods for inverter-based microgrids [15], impacts of distributed energy resources on UFLS schemes [16], and UFLS performance under IBR integration in the Western Interconnection [17]. Regarding high-bandwidth controls, studies have shown the potential favorable impact of high-bandwidth on UFLS performance [4] and the capability of high-bandwidth energy storage systems (ESS) in providing frequency regulation to prevent widespread load-shedding events [18], [19]. Additional research has implemented UFLS strategies to support frequency recovery with high inverter penetration [20]. Industry reports have emphasized the need for standardizing inverter capabilities, particularly regarding inertia support and frequency response [21]. Overall, existing studies show that the high-bandwidth IBR is advantageous in frequency recovery, improving the performance of the UFLS scheme. While existing studies demonstrate high-bandwidth IBRs' advantages

979-8-3315-8138-1

in frequency recovery and UFLS performance, significant knowledge gaps remain regarding comparative analyses of UFLS under SG and high-bandwidth IBR integration, as well as the impacts of high-bandwidth control settings on frequency dynamics and legacy UFLS schemes.

To address these knowledge gaps, this paper investigates UFLS schemes in IBR-integrated systems with various controls through:

- Electromagnetic transient (EMT) modeling of a modified North American transmission system with SG and IBR
- Comparative studies on the UFLS scheme in systems with IBR and SG
- Performance of the UFLS scheme with varying IBR control strategies and settings
- Limitations of IBRs in UFLS

II. Basic Knowledge of High-Bandwidth control and UFLS

In the typical high-bandwidth IBR control structure, PSL and reactive power droop (Q droop) control regulate the magnitude and angle of internal voltage vectors. In high-bandwidth controls, PSLs regulate the angular frequency according to:

$$\begin{cases} \omega = \frac{d_\omega}{J_v s + d_\omega}\omega^* + \frac{G_P(s)}{J_v s + d_\omega}(P^* - P) & \text{VSM} \\ \omega = \omega^* + d_P G_P(s)(P^* - P) & \text{droop} \\ \omega = \omega^* + \frac{\omega^* \kappa_1 G_P(s)}{(V^{d*})^2}(P^* - P) & \text{dVOC} \end{cases} \quad (1)$$

where superscript * denotes reference values, $\{\boldsymbol{V}, \boldsymbol{I}\}$: AC side voltages and currents, $\{\theta, \omega\}$: orientation angle and angular frequency. $P = V^d I^d + V^q I^q$. J_v represents virtual inertia constant, κ_1 is synchronization control gain, d_ω denotes frequency damping coefficient and d_P is active power damping coefficient. The low-pass filter is given by $G_P(s) = \omega_f/(s+\omega_f)$. Considering $\frac{d_\omega}{(J_v s + d_\omega)} \approx 1$, the frequency deviation $\Delta\omega$ is expressed as

$$\Delta\omega = \omega - \omega^* \approx \frac{D_P}{Js + D_\omega}(P^* - P) \quad (2)$$

where $\{D_P, J, D_\omega\}$ represent equivalent active power damping, virtual inertia, and frequency damping. Table I presents the approximate computation of these equivalent parameters from PSL parameters.

TABLE I
Equivalent Parameters of High-Bandwidth IBR

Parameters	VSM	Droop	dVOC
D_P	1	d_P	$\frac{\omega^*\kappa_1}{(V^{d*})^2}$
J	J_v	$\frac{1}{\omega_f}$	$\frac{1}{\omega_f}$
D_ω	d_ω	1	1

PSL parameter tuning affects IBRs' equivalent damping and inertia, influencing frequency dynamics and resilience. The active power droop mechanism determines frequency deviation, which directly impacts load shedding executed by UFLS relays at designated substations. After sufficient load shedding, the frequency increases and stabilizes at a new steady state. For system security, UFLS schemes must maintain frequency below permissible instantaneous over-frequency trip thresholds [4] (e.g., 61.8 Hz for the Eastern Interconnection (EI) [22] per NERC PRC-024 [10]). If UFLS action is inadequate to recover the frequency, the decline will persist, potentially leading to generator trips and a blackout. Inadequate UFLS response can lead to persistent frequency decline, potentially triggering generator trips and system blackouts. The following case studies will further analyze IBR control impacts on UFLS performance.

III. Test System and Simulation Results

A. Test System Configuration

The UFLS test system, representing a portion of a modified North American transmission system with an external system within the EI, is built in EMT domain, as shown in Fig. 1. Table II presents generator data. G15 and G16 represent the equivalent source of the rest of the system and consist of two 1000 MVA generators that have been represented by an equivalent machine with an inertia of 6.22 s and no governor model. The internal generation model (G3, G4, G6, G13, and G14) includes a machine with inertia values in Table II, an exciter, and a governor model. The simulated UF event is the tripping of G14.

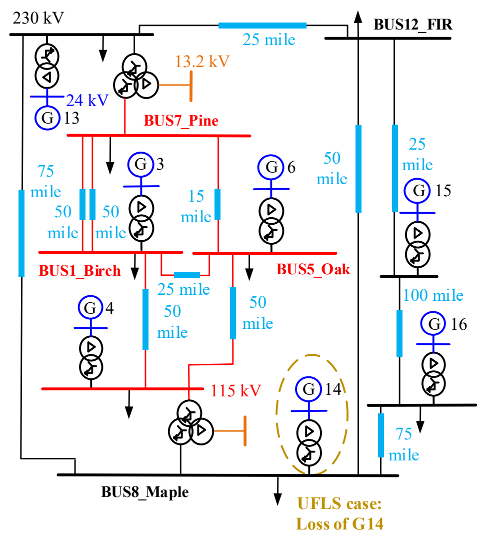

Fig. 1. Modified North American transmission system for UFLS test.

TABLE II
Generator Data in UFLS Test System

Generator	G3	G4	G6	G13	G14	G15	G16
Nameplate MVA	150	100	100	300	500	1000	1000
Inertia (s)	6.22	6.22	5.48	3.33	2.24	3.96	3.96

TABLE III
UFLS Levels and Percentage of Load Shedding

UFLS Level	1	2	3
Freq (Hz)	59.3	59	58.7
Percent of Peak Load Shed (%)	12.5	12.5	12.5
Load Shed with 6-Cycle Delay (MW)	150	150	150
Load Shed with 30-Cycle Delay (MW)	100	100	100
Total Load Shed (MW)	250	250	250

In the test system, the peak load is 2100 MW. Table III presents UFLS levels, percentage of load shedding, loads with 6-cycle delay, and loads with 30-cycle delay [23]. Load shedding is carried out by UFLS relays at designated load substations, which activate a lockout relay to disconnect the load. These load substations are listed in Table IV. The IBR

979-8-3315-8138-1

model employed herein is a generic type. For example, an aggregated IBR model can be utilized to substitute G16, with the total number of IBR generation units set to match the power of a conventional generator.

TABLE IV
LOAD SHEDDING AT DESIGNATED LOAD SUBSTATIONS

Level	Delay (cyc)	Load (MW)	Substation
1	6	150	Pine
	30	75	Oak
	30	25	Birch
2	6	75	FIR
	6	75	FIR
	30	50	Oak
	30	50	Maple
3	30	25	Birch
	6	75	Maple
	6	75	Maple
	30	75	Oak

B. Performance in different generator scenarios

To investigate the impacts of generator type on the UFLS scheme, the response of the UFLS scheme has been compared under three different generator scenarios: (i) Scenario 1 where all generators of the test system are conventional SGs, (ii) Scenario 2 where 27% of the total MW generation (G16) has been replaced by low-bandwidth IBRs, (iii) Scenario 3 where 27% of the total MW generation has been replaced by high-bandwidth IBRs with VSM control. Table V presents the parameters of PLL and PSL in this paper. The low-bandwidth IBR employs a conventional PLL with a PI regulator to obtain the frequency reference. The fast frequency response (FFR) capability of low-bandwidth IBRs has not been considered.

TABLE V
PARAMETERS OF PLL AND PSL

Parameter	Value	Equivalent parameter value (D_P, J, D_ω)
VSM control (J_v, d_ω)	0.15, 0.8038	(1, 0.15, 0.8038)
droop control (d_P, ω_f)	1.244, 125.6	(1, 0.0064, 0.8038)
dVOC (κ_1, ω_f)	0.0033, 125.6	(1, 0.0064, 0.8038)
PI parameters (PLL)	7.5, 300	NA

TABLE VI
UFLS TRIP IN DIFFERENT GENERATOR SCENARIOS

Level	Substation	Time (s)		
		All SG	27% low-bandwidth	27% high-bandwidth
1	Pine	21.19	21.01	23.76
	Oak	21.59	21.42	24.16
	Birch	21.59	21.42	24.16
2	FIR	21.52	21.29	NA
	Oak	21.92	21.68	NA
	Maple	21.92	21.68	NA
3	Birch	NA	22.11	NA
	Maple	NA	21.71	NA
	Oak	NA	22.11	NA
Total load shedding (MW)		500	750	250

In the UFLS test, Fig. 2 and Fig. 3 compare the simulation results of system frequency and RoCoF in the three generator scenarios, and Table VI shows the time that each UFLS level is tripped and the total load shedding in different scenarios. Fig. 4 shows the active power outputs of G16 and G3. G16 is replaced by SG, low-bandwidth IBR, and high-bandwidth-IBR in the three generator scenarios, respectively. G3 is an SG with an exciter and governor model.

For scenario 1 (All SG), UFLS levels 1 and 2 trip, thus shedding a total of 500 MW of system load. Following the UFLS operation, the frequency increases and settles out at a value of about 60.4 Hz. This value is below the allowable instantaneous over-frequency tripping value of 61.8 Hz. Thus, no further generator outage is expected.

For scenario 2 (27% low-bandwidth IBR), the RoCoF just after the UF event increases significantly, as shown in Fig. 3. From Fig. 4, the low-bandwidth IBR is not involved in power regulation, deteriorating the power outputs of other SGs in the test system. During t=20 s−22 s, the decreasing frequency leads to the tripping of the UFLS level 3 with a total of 750 MW load shed. The frequency rebound exceeds 61.8 Hz, thus indicating that over-frequency generation tripping may occur.

For scenario 3 (27% high-bandwidth IBR), following the UF event at t=20 s, the system frequency starts to decrease, and the high-bandwidth IBR increases its injected active power, emulating the active power response of SGs. The outcome is that the frequency decline is arrested, and the frequency is stabilized at 59.25 Hz, just below UFLS level 1. This results in the tripping of UFLS level 1 and shedding of 250 MW load on substations Pine, Oak, and Birch, as shown in Table VI. UFLS level 2 and level 3 are not tripped. The study indicates that high-bandwidth IBR demonstrates a P-f droop mechanism similar to that of SGs, which helps address potential misoperations of UFLS caused by low-bandwidth IBR.

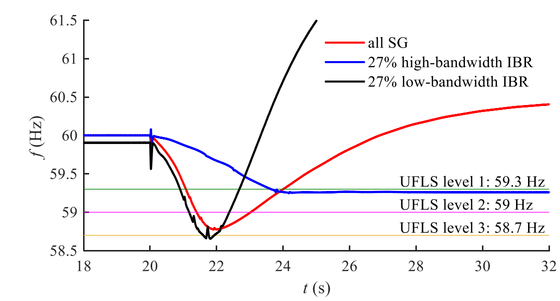

Fig. 2. System frequency in different generator scenarios for the UFLS test.

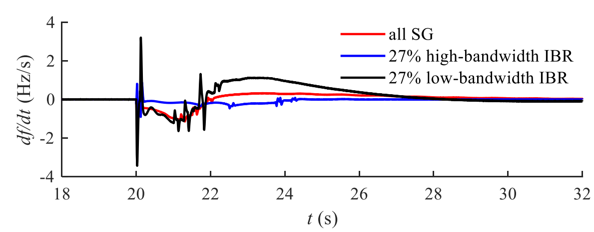

Fig. 3. RoCoF in different generator scenarios for the UFLS test.

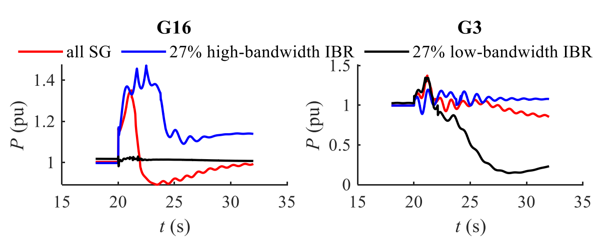

Fig. 4. Active power outputs in different generator scenarios for UFLS test.

C. Performance under different high-bandwidth controls

In different high-bandwidth control modes, Fig. 5 and Fig. 6 compare the UFLS test results, and Table VII shows the time that each UFLS level is tripped. As shown, high-bandwidth control modes impact the system frequency, RoCoF, and power

979-8-3315-8138-1

outputs. In Table V, high-bandwidth IBRs have been parameterized to facilitate straightforward comparison. The droop control and dVOC have the same equivalent parameters $\{D_P, J, D_\omega\}$, so their frequency and power dynamics are almost consistent. The equivalent virtual inertia of VSM control is larger than that of droop control and dVOC, extending the settling time of frequency responses. These results suggest that the performance of UFLS is primarily determined by IBR control parameters. This will be further analyzed subsequently.

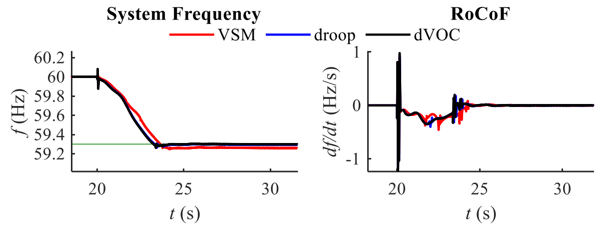

Fig. 5. Frequency responses in different high-bandwidth control modes for UFLS test.

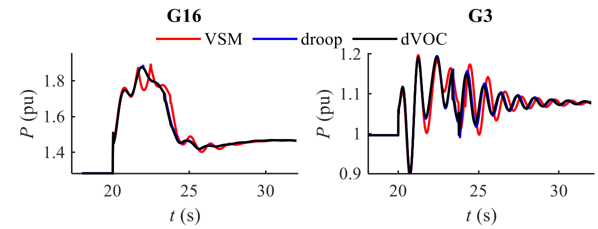

Fig. 6. Active power outputs in different high-bandwidth control modes for UFLS test.

TABLE VII
UFLS TRIP IN DIFFERENT HIGH-BANDWIDTH CONTROL MODES

Level	Substation	Time (s)		
		VSM	Droop	dVOC
1	Pine	23.76	23.42	23.36
	Oak	24.16	23.82	23.76
	Birch	24.16	23.82	23.76

D. Performance under different control settings

The equivalent damping and inertia of IBRs impact the frequency dynamics and resilience. Fig. 7 shows that a larger J leads to a slower decline in frequency and a lower frequency nadir, extending the tripping time of loads in Table VIII. The power oscillation becomes more significant under a larger J, as shown in Fig. 8. Fig. 9 shows that a larger D_ω leads to a slower decline in frequency and a higher frequency nadir, extending the tripping time of loads. The power oscillation is smaller under a larger D_ω, as shown in Fig. 10. Fig. 11 shows that a larger D_P leads to a faster decline in frequency and a lower frequency nadir, shortening the tripping time of loads. In Fig. 12, the power oscillation is reduced under a larger D_P.

TABLE VIII
UFLS TRIP UNDER VARYING $\{J, D_\omega, D_P\}$

Level 1		Substation		
		Pine	Oak	Birch
Time (s)	J=0.015	23.44	23.84	23.84
	J=0.15	23.76	24.16	24.16
	J=1.5	24.78	25.18	25.18
	D_ω=0.4	22.55	22.95	22.95
	D_ω=0.6	23.08	23.48	23.48
	D_ω=0.8	23.76	24.16	24.16
	D_P=0.4	23.42	23.82	23.82
	D_P=0.6	22.85	23.24	23.24
	D_P=0.8	22.41	22.81	22.81

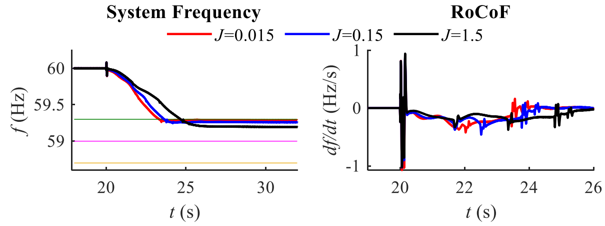

Fig. 7. System frequency under varying J for the UFLS test.

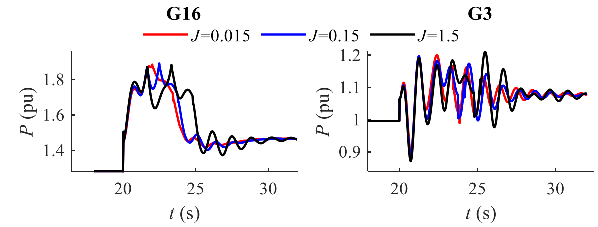

Fig. 8. Active power outputs of G16 under varying J for the UFLS test.

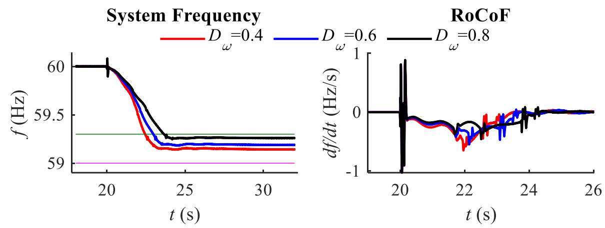

Fig. 9. Frequency responses under varying D_ω for the UFLS test.

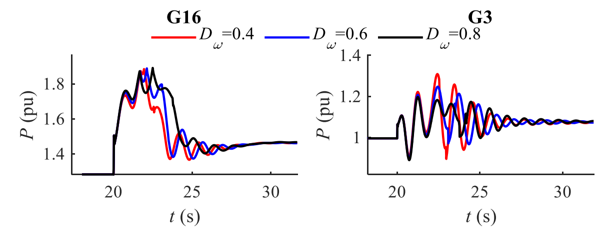

Fig. 10. Active power outputs under varying D_ω for the UFLS test.

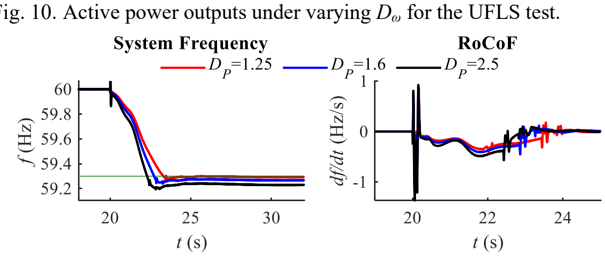

Fig. 11. System frequency under varying D_P for the UFLS test.

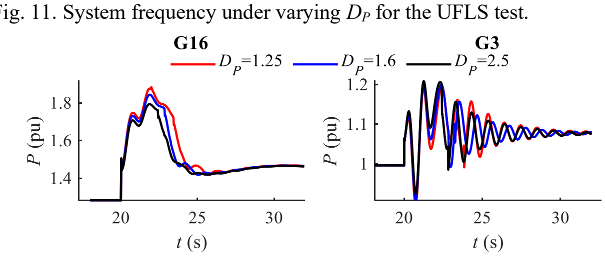

Fig. 12. Active power outputs of G16 under varying D_P for the UFLS test.

E. System Instability case with IBR

While adjusting equivalent inertia and damping of IBRs can alter the frequency regulation, they cannot be freely adjusted to achieve the desired dynamic response and frequency nadir, as this could jeopardize system stability. Fig. 13 and Fig. 14 show the diverging frequency and power outputs when J=0.005 and D_ω=1.2. During t = 20 s −21.66 s, the frequency decreases while the IBR injects active power into the grid. When t=21.66 s, the converter currents reach the current limit of 1.2 pu, as shown in

979-8-3315-8138-1

Fig. 13. Consequently, the IBR cannot provide more active power to support the frequency, resulting in the divergence of the frequency response and power output. When t=23.44 s, the level 1 of UFLS trips, leading to system instability. Overall, these results suggest that the limitation of IBR: (i) Selection of IBR control parameters considering only UFLS might compromise system stability. (ii) When the power capacity of IBRs fails to compensate for a generator loss, the frequency response and power output would diverge.

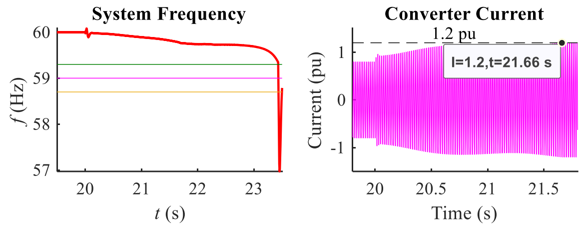

Fig. 13. System frequency and Phase A converter when J=0.005 and D_ω=1.2.

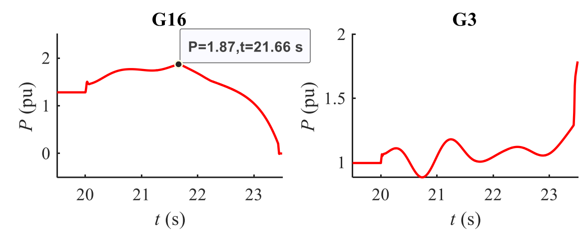

Fig. 14. Active power outputs of G16 when J=0.005 and D_ω=1.2.

IV. Conclusions

This paper has examined the performance of UFLS schemes in a modified North American transmission system featuring both SGs and IBRs with various control strategies. Our EMT simulation results reveal that the integration and control of IBRs significantly influence system stability and UFLS reliability. Low-bandwidth IBRs using conventional PLLs can increase the RoCoF after disturbances, risking excessive load shedding and generator tripping. In contrast, high-bandwidth IBRs, especially those with virtual inertia and optimized damping controls, can mitigate these issues and improve UFLS operation.

The system's frequency response is highly dependent on IBR control parameters: larger virtual inertia and frequency damping, combined with appropriate active power damping, can reduce frequency decline rates and power oscillations. However, while tuning these parameters enhances frequency regulation, unrestricted adjustment may compromise system stability. Additionally, IBRs are limited by converter current capacity, which constrains their ability to compensate for generator loss. Insufficient active power support from IBRs can result in inadequate frequency recovery and unstable power output.

Overall, careful consideration of available active power, control bandwidth, and parameter settings is essential for integrating IBRs into existing grids and ensuring reliable UFLS performance as power systems evolve.

V. References

[1] S. Bustamante, J. W. gonzález, G. J. López *et al.*, "UFLS and Smart Load for Frequency Regulation in Electrical Power System: A Review," *IEEE Access,* vol. 11, pp. 110967-110984, 2023.
[2] I. Manamperi, I. Ahmad, D. Habibi *et al.*, "Assessing the Effects of Low Load on Under-Frequency Load Shedding Schemes and Exploring Potential Solutions: A Review," 2023 International Conference on Sustainable Technology and Engineering (i-COSTE), 2023.
[3] A. Haddadi, Impact of Grid-Forming Inverter on System Protection, IEEE PES GM 2024 Panel on Protection Challenges in the Decarbonized and Resilient Power Grid, Seattle WA, USA, July 2024.
[4] *Investigation of Grid Forming Inverter Fault Response and its Impact on System Protection*— Technical Update. EPRI, Palo Alto, CA: 2024. 3002024262.
[5] C. O'Malley, L. Badesa, F. Teng *et al.*, "Probabilistic scheduling of UFLS to secure credible contingencies in low inertia systems," *IEEE Trans. Power Syst.*, vol. 37, no. 4, pp. 2693–2703, Jul. 2022.
[6] U. Markovic, O. Stanojev, P. Aristidou *et al.*, "Understanding Small-Signal Stability of Low-Inertia Systems," *IEEE Trans. Power Syst.*, vol. 36, no. 5, pp. 3997-4017, Sept. 2021.
[7] P. Sun, Z. Tian, M. Huang *et al.*, "Additional Kinetic Energy Injection and Piecewise Damping Based Postfault Anti-Windup and Transient Stability Enhanced Control for Grid-Forming Inverter," *IEEE Trans. Power Electron.,* pp. 1-15, 2024.
[8] E. A. S. Ducoin, Y. Gu, B. Chaudhuri *et al.*, "Analytical Design of Contributions of Grid-Forming and Grid-Following Inverters to Frequency Stability," *IEEE Trans. Power Syst.,* vol. 39, no. 5, pp. 6345-6358, 2024.
[9] T. Amraee, M. G. Darebaghi, A. Soroudi *et al.*, "Probabilistic under frequency load shedding considering RoCoF relays of distributed generators," *IEEE Trans. Power Syst.*, vol. 33, no. 4, pp. 3587–3598, Jul. 2018.
[10] NERC, SPP "Automatic Underfrequency Load Shedding: PRC-006- SPP-01." [Online]. Available: http://www.nerc.com/docs/standards/rrs/ SPP UFLS Regional Standard Draft%207 clean.pdf
[11] H. Zhang, W. Xiang, W. Lin *et al.*, "Grid Forming Converters in Renewable Energy Sources Dominated Power Grid: Control Strategy, Stability, Application, and Challenges," *Journal of Modern Power Systems and Clean Energy,* vol. 9, no. 6, pp. 1239-1256, 2021.
[12] A. Tayyebi, D. Groß, A. Anta *et al.*, "Frequency Stability of Synchronous Machines and Grid-Forming Power Converters," *IEEE Trans. Emerg. Sel. Topics Power Electron.,* vol. 8, no. 2, pp. 1004-1018, 2020.
[13] Q. Hu, R. Han, X. Quan *et al.*, "Grid-Forming Inverter Enabled Virtual Power Plants With Inertia Support Capability," *IEEE Trans. Smart Grid,* vol. 13, no. 5, pp. 4134-4143, 2022.
[14] J. Wang and K. Ma, "Inertia and Grid Impedance Emulation of Power Grid for Stability Test of Grid-Forming Converter," *IEEE Trans. Power Electron.,* vol. 38, no. 2, pp. 2469-2480, 2023.
[15] E. Dehghanpour, H. K. Karegar, and R. Kheirollahi, "Under Frequency Load Shedding in Inverter Based Microgrids by Using Droop Characteristic," *IEEE Trans. Power Del.,* vol. 36, no. 2, pp. 1097-1106, 2021.
[16] A. Haddadi, E. Farantatos, P. Mitra *et al.*, "Impact of Distributed Energy Resources on Under Frequency Load Shedding," 2022 IEEE Power & Energy Society General Meeting (PESGM), 2022.
[17] D. Tucker, D. Kosterev, and A. Sajadi, "Frequency Response in the Western Interconnection with Significantly High Shares of Inverter-Based Resources: 100% Renewable Case," 2022 IEEE Power & Energy Society General Meeting (PESGM), 2022.
[18] I. Manamperi, I. Ahmad, D. Habibi *et al.*, "Optimising grid-forming inverters to prevent under-frequency load shedding with minimal energy storage," *Journal of Energy Storage,* vol. 98, 2024.
[19] A. B. Nassif, M. Rahmatian, A. Paaso *et al.*, "Improving Frequency Stability and Minimizing Load Shedding Events by Adopting Grid-Scale Energy Storage with Grid Forming Inverters," 2023 IEEE PES Innovative Smart Grid Technologies Latin America (ISGT-LA), 2023.
[20] O. D. Garzon, A. B. Nassif, M. Rahmatian *et al.*, "Frequency Stability Enhancement by Grid Forming Resources in Replicated Load Shedding Events," 2024 IEEE Power & Energy Society General Meeting (PESGM), 2024.
[21] J. Gui, H. Lei, T. R. McJunkin, and B. K. Johnson, "Frequency Resilience Enhancement for Power Systems with High Penetration of Grid-Forming Inverters," 2023 IEEE Power & Energy Society Innovative Smart Grid Technologies Conference (ISGT), 2023.
[22] R. Yousefian, X. Xu, M. Elkhatib *et al.*, "Benchmarking and Simulation of Frequency Events in the Eastern Interconnection," 2022 IEEE Power & Energy Society General Meeting (PESGM), 2022.
[23] Jones, K. W., Webber, K., & Bhuvaneshwaran, K. "The need for faster underfrequency load shedding," in Proc. 74th Annu. Conf. Protective Relay Eng., Virtual, Mar. 22–25, 2021.

979-8-3315-8138-1